

## Mixed Linkers

# A Simple and Non-Destructive Method for Assessing the Incorporation of Bipyridine Dicarboxylates as Linkers within Metal–Organic Frameworks

Christopher H. Hendon,<sup>[a, b]</sup> Jonathan Bonnefoy,<sup>[c]</sup> Elsje Alessandra Quadrelli,<sup>[d]</sup> Jerome Canivet,<sup>[c]</sup> Matthew B. Chambers,<sup>[e]</sup> Gwenaëlle Rousse,<sup>[f]</sup> Aron Walsh,<sup>[a]</sup> Marc Fontecave,<sup>[e]</sup> and Caroline Mellot-Draznieks<sup>\*[e]</sup>

**Abstract:** As a novel avenue for applications, metal–organic frameworks (MOFs) are increasingly used for heterogenizing catalytic molecular species as linkers into their crystalline framework. These multifunctional compounds can be accessed with mixed linkers synthesis or postsynthetic-exchange strategies. Major limitations still reside in their challenging characterization; in particular, to provide evidence of the genuine incorporation of the functionalized linkers into the framework and their quantification. Herein, we demonstrate that a combination of computational chemistry, spectroscopy and X-ray diffraction allows access to a non-destructive analysis of mixed-linker UiO-67-type materials featuring biphenyl- and bipyridine-dicarboxylates. Our UV/Vis-based methodology has been further applied to characterize a series of Rh-functionalized UiO-67-type catalysts. The proposed approach allows a recurrent key issue in the characterization of similar supported organometallic systems to be solved.

Metal–organic frameworks (MOFs) are attracting ongoing exceptional interest in the scientific community since they demonstrated their wide chemical and structural versatility<sup>[1]</sup> as well as efficacy in high-value-added applications for energy, fine chemicals synthesis or health care. In the particular field of photocatalysis, MOFs are reported to be very promising materials thanks to their porous and hybrid organic–inorganic structure allowing the fine-tuning of their light-harvesting and cata-

lytic properties.<sup>[2]</sup> Among the large range of available MOFs, the zirconium-based frameworks, such as the UiO-6n ( $n=6,7,8$ ) series are now widely studied platforms for heterogeneous photocatalytic systems stemming from their ease of synthesis and functionalization associated with their exceptional chemical and thermal stability under realistic conditions.<sup>[3]</sup> Furthermore, a variety of isoreticular Zr–UiO structures are accessible using isotopological organic ligands with various lengths and functional groups as linkers.<sup>[4]</sup> Of particular interest, 2,2'-bipyridinedicarboxylate (bipydc) is isotopological to the ubiquitous biphenyldicarboxylate (bpdc) linker, and 2,2'-bipyridine (bipy) is extensively used as an organic ligand for chelating active molecular metal complexes, the widely used photosensitizer [Ru(bipy)<sub>3</sub>Cl<sub>2</sub>] being the most known example.

Lin and co-workers previously demonstrated the efficiency of Zr–UiO-67 solids self-assembled using a series of organometallic complexes, such as Re-, Ir- and Ru–bipydc linkers, for various photocatalytic reactions.<sup>[3f]</sup> More generally, the incorporation of bipydc derivatives as linkers within the primarily bpdc-based Zr–UiO-67 solid provides a foundation for building new MOF-based photocatalytic systems,<sup>[5]</sup> using either mixed-linker (ML) synthesis or post-synthetic exchange (PSE) strategies. Still, the in-depth characterization of such solids containing multiple linkers, that is, mixed-linker MOFs or MOF-supported organometallic complexes, remains a challenge which must be addressed in order to rule out a simple, even if irreversible, encapsulation of the organic ligand and provide evidence for the genuine incorporation within the hybrid framework. Indeed, whether the MOF acts as a cooperative solid ligand or as an electronically neutral nano-container is of a par-

[a] Dr. C. H. Hendon, Prof. A. Walsh  
Department of Chemistry, University of Bath, Claverton Down  
Bath, BA2 7AY (UK)

[b] Dr. C. H. Hendon  
Department of Chemistry, Massachusetts Institute of Technology  
77 Massachusetts Ave., Cambridge, MA (USA)


[c] J. Bonnefoy, Dr. J. Canivet  
IRCELYON  
Institut de Recherche sur la Catalyse et l'Environnement de Lyon  
Univ. Lyon 1 - UMR CNRS 5256, 2 av. A. Einstein  
69626 Villeurbanne (France)

[d] Dr. E. A. Quadrelli  
C2P2, Univ. Lyon 1 - UMR CNRS 5265, CPE Lyon  
43 Bd du 11 Novembre 1918 69616, Villeurbanne (France)

[e] Dr. M. B. Chambers, Prof. M. Fontecave, Dr. C. Mellot-Draznieks  
Laboratoire de Chimie des Processus Biologiques  
UMR 8229 CNRS, UPMC Univ Paris 06  
Collège de France, 11 Place Marcelin Berthelot, 75231, Paris (France)

[f] Dr. G. Rousse  
FRE 3677 "Chimie du Solide et Energie", Collège de France  
11 Place Marcelin Berthelot, 75231 Paris Cedex 05, (France)  
and  
UPMC Univ Paris 06, Sorbonne Universités, 4 Place Jussieu, 75005 Paris (France)

 Supporting information and ORCID(s) from the author(s) for this article are available on the WWW under <http://dx.doi.org/10.1002/chem.201600143>.

 Part of a Special Issue "Women in Chemistry" to celebrate International Women's Day 2016. To view the complete issue, visit: <http://dx.doi.org/chem.v22.11>.

amount importance to understand photocatalytic mechanisms and for further improving MOF-based systems.

To date, diagnosing the incorporation of the bipydc linker within the Zr-UiO-67s framework remains complicated, considering that the structural information in UiOs is often limited to the analysis of the X-ray powder pattern in combination with spectroscopic techniques (IR spectroscopy, extended X-ray absorption fine structure (EXAFS), etc).<sup>[4a,6]</sup> Only recently, a structural analogue of Zr-UiO-67 was prepared with bipydc and its structure solved using single-crystal data,<sup>[7]</sup> providing a clear insight into the post-synthetic metalation of this solid.<sup>[8]</sup> In principle, solid-state NMR potentially allows such in-depth characterization of multiple linkers in MOFs. Recently sophisticated approaches, including rotational-echo double-resonance (REDOR) NMR measurements combined with Monte Carlo simulations<sup>[9]</sup> and  $H^1$  spin-diffusion magic-angle spinning measurements<sup>[10]</sup> provided detailed information on the apportionment of multiple linkers within the MOF-5 crystal structure. We applied dynamic nuclear polarization (DNP) NMR techniques to post-synthetically functionalized MOFs, determining the distribution of different linkers inside a unique framework.<sup>[11]</sup> Still, such NMR methods are rather time-consuming and limited to diamagnetic systems that suffer from potentially long relaxation times.<sup>[12]</sup>

Recently, we reported the heterogenization of a molecular rhodium catalyst,  $[Cp^*Rh(bipydc)]$  ( $Cp^* = C_5Me_5$ , by postsynthetic linker exchange in Zr-UiO-67 to build the  $Cp^*Rh@UiO-67$  catalyst designed to perform the photoreduction of  $CO_2$  into formate.<sup>[13]</sup>

At the time, the incorporation of the  $[Cp^*Rh(bipydc)]$  metal complex as a linker within the UiO's framework was proved using indirect evidence combining an NMR-monitored functionalization reaction, elemental analysis, X-ray powder diffraction and gas sorption. This time-consuming procedure, while in strong support of the postulated Rh-functionalized Zr-UiO-67 structure, mostly based its characterization of the covalent incorporation of the  $[Cp^*Rh(bipydc)]$  complex within the framework on indirect evidence.

Herein, we present an easily accessible method to assess and quantify the genuine incorporation of two linkers, bpdc and bipydc, into a single MOF crystal structure, using the topical Zr-UiO-67 MOF as a case study. Our non-destructive approach is constructed around the symbiosis of accessible computational chemistry, UV/vis spectroscopy and crystallography. In the first step, DFT calculations determined changes in both the electronic and crystal structures of Zr-UiO-67 upon the incorporation of the bipydc linker within the framework. Both UV/vis and X-ray diffraction were used to corroborate the calculation findings on a series of mixed-linker Zr-UiO-67 solids (Figure 1a) featuring various bpdc/bipydc compositions. In a second step, we analysed the UV/vis spectra of the  $Cp^*Rh@UiO-67$  series of solids (Figure 1b) synthesized using a postsynthetic-exchange strategy.<sup>[13]</sup> With the methods presented herein, we ascertain with certainty that the incorporation of the  $[Cp^*Rh(bipydc)]$  complex into the functionalized Zr-UiO-67 framework, and more generally, has led to the development of a method of analysis of ligand uptake in metal-organic frameworks that features mixed-linker functionality.

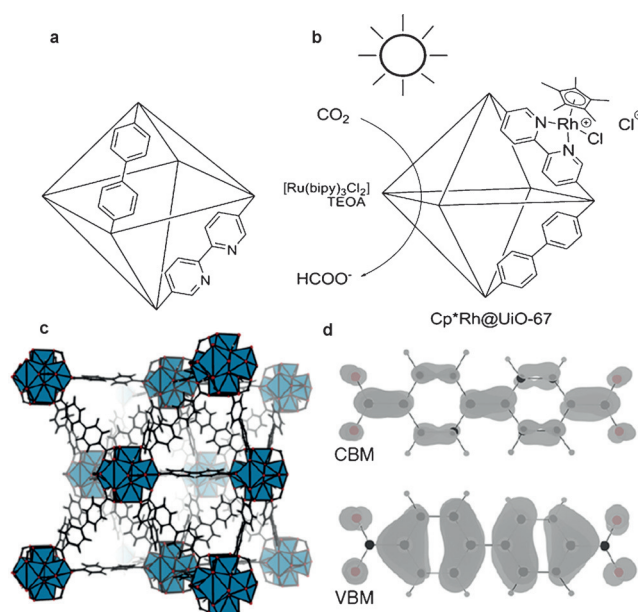


**Figure 1.** Schematic representation of a) the crystal structure of the mixed-linker Zr-UiO-67 featuring bpdc and bipydc linkers and b) of the  $Cp^*Rh@UiO-67$  catalyst featuring the  $[Cp^*Rh(bipydc)]$  complex as a linker.<sup>[13]</sup> c) Pristine Zr-UiO-67. d) Conduction band minimum (CBM) and valence band maximum (VBM) of the bpdc linker in the pristine Zr-UiO-67.

DFT calculations were performed for a series of mixed-linker Zr-UiO-67-based models. The reported defect-free crystallographic structure of the pristine bpdc-based Zr-UiO-67 (Figure 1c) was used for the all DFT calculations, featuring six distinct bpdc linkers in its primitive cell.<sup>[14]</sup> As a result, substitutions of bipydc may be made in 16% increments. Considering these substitutions, seven models were constructed: Zr-UiO-67,<sup>[14]</sup> Zr-UiO-67-16% bipydc, Zr-UiO-67-33% bipydc, Zr-UiO-67-50% bipydc, Zr-UiO-67-66% bipydc, Zr-UiO-67-83% bipydc and Zr-UiO-67-100% bipydc. The seven structures were relaxed with respect to lattice parameters and atomic positions by using the PBEsol functional in VASP<sup>[15]</sup> with the convergence criteria detailed in the Supporting Information. The resultant structures were found to be in excellent agreement with experimentally collected data. A long-range screen hybrid functional, HSE06<sup>[16]</sup> was also employed to recover quantitative electronic properties.

The computed changes in cell volume and band gap as a function of the bipydc composition are presented in Figure 2a (PBEsol) and b (HSE06), revealing a cell contraction correlated to a band-gap closure. The HSE06-computed band gaps were consistently 1.2 eV greater than those predicted by PBEsol, thus correcting the systematic underestimation from PBEsol. The HSE06-computed Zr-UiO-67 electronic band gap (3.63 eV) is in excellent agreement with the measured optical band gap (3.5–3.68 eV).<sup>[6b]</sup> The marked similarities between the functionals provide two productive avenues for broadening the scope of our methods: 1) PBEsol performs systematically similar to HSE06 with the deficit of recovering quantitative electronic properties. However, qualitatively PBEsol was indeed useful, and required substantially less computational resources.

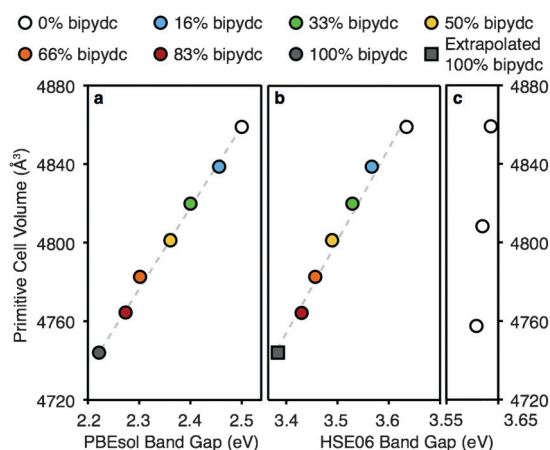


**Figure 2.** The linear correlation between computed primitive cell volume of Zr-UiO-67-%bipydc models and the PBEsol (a) and HSE06 (b) electronic band gap. The extrapolated value for HSE06 Zr-UiO-67-100% bipydc (grey square) is derived from the line of best fit to overcome the computational limitation. To elucidate whether lattice contraction alone can be attributed to the reduction in band gap, explicit calculations of cell contraction of the native Zr-UiO-67 were performed (c), and show that the reduction in band gap is not explicitly a product of reduced cell volumes.

2) We struggled to obtain sufficient electronic convergence for the 100% bipydc model, and hence confidently extrapolated to this point in Figure 2b (grey square) on the basis of PBEsol data.

From these substitution-induced lattice contractions and band-gap reductions, two interesting questions arise: 1) What is the origin of the band-gap reduction and 2) what is the origin of the lattice contraction. These questions cannot be answered exclusive of each other. Expectedly, the band edges of UiO-67 and its derivatives are defined by the organic linker.<sup>[6b,13,17]</sup> The highest-occupied state (Figure 1d) is centred on bpdc, regardless of the bipydc composition (see 50% bipydc example in Figure S1, Supporting Information). However, the lowest-unoccupied state shifts from being bpdc-centred in the pristine Zr-UiO-67 as shown in Figure 1d to primarily bipydc-centred in all bipydc-containing models.

This slight reduction in the conduction-band minimum (CBM) energy results in a decrease in the band gap. Furthermore, as the amount of bipydc per cell increases, the gap closes as the band-edge energy decreases with increased DOS at the CBM. The localization of the CBM for the Zr-UiO-67-50% bipydc model is shown in Figure S1b, Supporting Information, and the projected DOS in Figure S2, Supporting Information. Thus, we can address one contributing origin to the observed band-gap decrease: a reduction in CBM energy and localization on bipydc.

To isolate the change in electronic properties arising from purely mechanical lattice contraction installed by the incorporation of bipydc, the pristine bpdc-based Zr-UiO-67 solid was compressed to pressures that produced similar cell volumes to those observed in bipydc-containing models (see the Supporting Information for details), as illustrated in Figure 2c.<sup>[18]</sup> Under the regime presented here, the increase in cell pressure (hence the reduced cell volume) alone produces a marginal redshift in

the electronic band gap and cannot account for the magnitude of the redshift predicted for the mixed-linker Zr-UiO-67s upon bpdc/bipydc exchange.<sup>[19]</sup>

The cell contraction (~2.3% with respect to the pristine Zr-UiO-67) is attributed to the decreased length of the bipydc linker relative to bpdc, that is, 9.92 versus 10.07 Å when measured from the terminal carbon atoms, and also to a smaller aromatic torsion angle (29.25 vs. 31.04°). Also, a subtle rotation of the inorganic ZrO<sub>2</sub> nodes connecting bipydc and bpdc linkers allows an incremental cell contraction upon bipydc incorporation.

We concluded that the decrease in band gap observed upon the substitution of bpdc with bipydc originates from a primarily chemical feature (rather than mechanical). Whilst both cell contraction and orbital energy tuning contribute to this effect, the latter is dominant. Importantly, the incorporation of bipydc within the Zr-UiO-67s framework should produce a detectable contraction in cell volume concomitant with a redshift in optical absorption.

To probe the predicted lattice contraction, a series of mixed-linker Zr-UiO-67s were synthesized so as to experimentally characterize the effect of increasing %bipydc compositions within the framework. The compounds were prepared according to the previously reported solvothermal self-assembly procedures.<sup>[4d,8a]</sup> The mixed-linker Zr-UiO-67 compounds were prepared by replacing part of the bpdc acid molecules with bipydc acid molecules in the synthetic mixtures. The synthesized solids featured 0, 13, 20, 46 and 100% bipydc linker, named Zr-UiO-67, Zr-UiO-67-13% bipydc, Zr-UiO-67-20% bipydc, Zr-UiO-67-46% bipydc and Zr-UiO-67-100% bipydc referring to the % of bipydc as measured by liquid <sup>1</sup>H NMR analysis of the dissolved samples (Figure S3, Supporting Information). The crystals were evacuated overnight at 120 °C under primary vacuum. Nitrogen adsorption isotherms revealed a slight decrease of the accessible surface areas with increasing %bipydc (Figure S4, Supporting Information).

The X-ray powder diffraction patterns of all samples confirmed the systematic retention of the crystalline framework, with no loss of crystallinity upon increasing %bipydc. Bragg peaks can be perfectly indexed with a cubic unit cell, with space-group *F*23, with no sign of secondary phase (Figure S5, Supporting Information). A gradual shift in  $2\theta$  positions when the amount of bipydc is increased indicates that the volume of the unit cell is gradually reduced as more bipydc is incorporated into the hybrid framework (Figure 3) by 135 Å<sup>3</sup> for the Zr-UiO-67-100% bipydc with respect to the pristine Zr-UiO-67, in line with the computational predictions (115 Å<sup>3</sup>). Lattice parameters (Table S2, Supporting Information) precisely follow the Vegard's law and this behaviour is, therefore, reminiscent of a solid solution behaviour between the two endmembers, the lattice parameters of which are in excellent agreement with those reported for the pristine Zr-UiO-67<sup>[14]</sup> and Zr-UiO-67-100% bipydc end members.<sup>[7]</sup>

We then turned to characterization with UV/vis spectroscopy of the synthesized mixed-linker Zr-UiO-67s series. Like most metal-organic frameworks, Zr-UiO-67 is a wide gap insulator with the pristine bpdc-based Zr-UiO-67 featuring an experi-

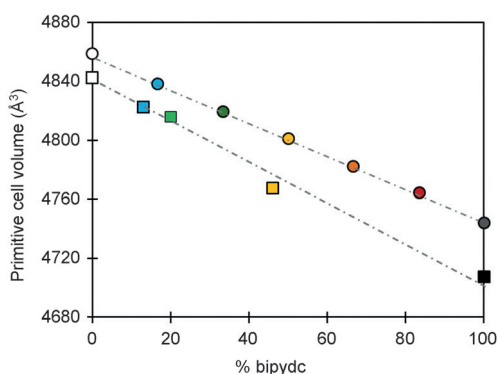


**Figure 3.** Experimental unit-cell volumes of the pristine Zr-UiO-67 and the series of Zr-UiO-67-% bipydc solids as a function of % bipydc (squares). Predicted cell volumes found from DFT calculations have been added (circles).

mental optical band gap of  $\sim 3.6$  eV.<sup>[6b]</sup> From the cell-volume contraction and computed band-gap reduction upon bipydc incorporation, it is anticipated that there should be a small but detectable redshift in the absorption onset. Figure 4 shows the experimental UV/vis absorption data obtained for the mixed-linker Zr-UiO-67-13% bipydc, -20% bipydc, -46% bipydc and -100% bipydc solids. The incorporation of bipydc into the Zr-UiO-67s crystal lattice not only causes an observable lattice contraction but also a redshifted UV/vis absorption spectrum. The gradient of the optical band gap closure as a function of bipydc incorporation within the hybrid framework follows a well-behaved linear regression in both calculations and experiments (Figure 4 inset,  $R^2=0.99$  and  $0.98$ , respectively). The slopes of the interpolation linear fit reported in the inset of Figure 4 are very similar for both calculations and experiment ( $-0.0018$  and  $-0.0024$  for the calculated and experimental series, respectively, individual band gap values being reported

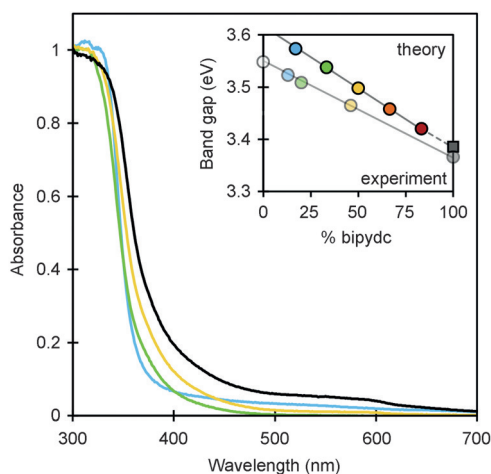


**Figure 4.** UV/vis absorption spectra of Zr-UiO-67-13% bipydc (blue), -20% bipydc (green), -46% bipydc (yellow) and -100% bipydc (black). The inset shows the reduction of the theoretical and measured band gaps as % bipydc increases (white circle refers to the pristine Zr-UiO-67 value reported in ref. [6b]). The theoretical value for the -100% bipydc solid (grey square) was derived by extrapolation from the PBEsol calculations trend (see the DFT section).

in Table S3, Supporting Information). In addition, the experimentally collected  $-100\%$  bipydc point corresponds very closely to that of our empirically derived  $-100\%$  bipydc model. This demonstrates that the exact amount of bipydc linker incorporated as a part of the Zr-UiO-67s framework can be monitored using the relative change in optical band gap values from the pristine to the targeted bipydc-functionalized MOF.

Finally, with the knowledge gleaned from the combination of DFT calculations, crystallographic and spectroscopic measurements, we can now address the issue of catalyst encapsulation versus framework incorporation through the measurement of the optical band gaps of post-synthetically bipydc-functionalized Zr-UiO-67s. Along this line, we considered the series of rhodium-containing Zr-UiO-67 catalysts, named Cp\*Rh@UiO-67s, that we reported as a stable heterogeneous system for the photocatalytic reduction of carbon dioxide into formate.<sup>[13]</sup> Following a postsynthetic-exchange strategy, a series of four solids, 5%-, 10%-, 20%- and 35%-Cp\*Rh@UiO-67, were prepared by reacting the pristine Zr-UiO-67 solid with the molecular complex [Cp\*Rh(bipydc)Cl<sub>2</sub>] to give the structures as schematically shown in Figure 1 b. Providing direct evidence of the incorporation of the Rh-functionalized bipydc linker into the Zr-UiO-67s framework by PSE is a key point. The diffuse reflectance spectra of the whole series of the Rh-containing Cp\*Rh@UiO-67s (Figure 5 a) allowed the determination of an optical band gap value of 2.4 eV assigned to the Rh-localized d-d transition and independent of the % [Cp\*Rh(bipydc)] composition. The intensity of this low-energy feature was found to increase as a function of the % [Cp\*Rh(bipydc)] composition. Originally unaddressed was the behaviour of the higher energy feature ( $\sim 3$  eV, indicated with an arrow Figure 5 a) assigned to the  $\pi$ - $\pi^*$  transition for the organic linkers within the MOF. We may now consider the evolution of this high-energy feature and observe its redshift as more [Cp\*Rh(bipydc)] linkers are introduced in the solid. Importantly the magnitude of this red shift is linearly correlated to the % [Cp\*Rh(bipydc)] and hence the amount of bipydc within the solid (Figure 5 b). Overall, despite the constant measured optical band gap of Zr-UiO-67 upon postsynthetic linker exchange (assigned to the lower-energy Rh-centred d-d transition), the shift of the higher energy  $\pi$ - $\pi^*$  transition may be interpreted in a similar fashion as in the series of Zr-UiO-67% bipydc solids as a signature of the genuine incorporation of the [Cp\*Rh(bipydc)]-functionalized linker within the framework.

Our simple and non-destructive way of characterizing the genuine incorporation of bipydc and bipydc-based metal complexes within the Zr-UiO-67s framework using UV/vis adsorption addresses a key issue in the characterization of MOF-supported organometallic systems. To this end, we have shown such an approach to be applicable with solids prepared either with mixed-linker synthetic strategy or postsynthetic exchange. In this instance, we explored the effects of multiple linkers on a framework constructed with Zr metal nodes—for which, the occupied *p*-orbitals and unoccupied *d*-orbitals shows certainly a negligible contribution to the band edges in MOFs that contain polyaromatic linkers. Most MOFs fulfil the criterion that either the valence band maximum (VBM) or conduction band

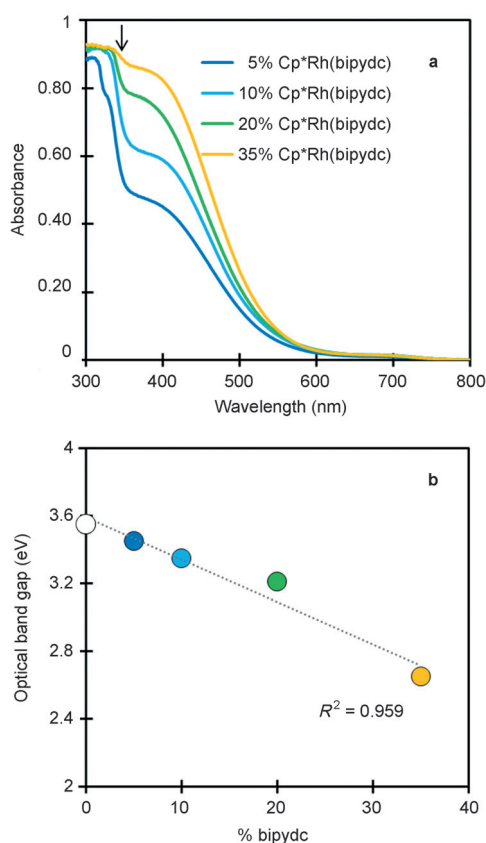


**Figure 5.** a) UV-vis absorption spectra of 5% (dark blue), 10% (cyan), 20% (green) and 35% Cp\*Rh@UiO-67 (yellow). The arrow indicates the  $\pi$ - $\pi^*$  transition of the organic linker. b) Experimentally measured optical band gap associated with the  $\pi$ - $\pi^*$  transition as a function of % [Cp\*Rh(bipydc)].

minimum (CBM) are controlled by organic  $\pi$ -electrons.<sup>[20]</sup> The application of our method may thus be broadened beyond Zr-UiO-67 and derivatives to any MOF featuring organic-centred frontier bands through the simple monitoring of the observable electronic transition associated to the linker (either in the UV or visible range). Such a combination of theory and experiment should provide a simple alternative to more complex and demanding characterization techniques, and an efficient pathway for the analysis of linkers' incorporation in metal-organic frameworks.

## Experimental Section

Computation, synthesis and characterization (PXRD, gas sorption, NMR) details are given in the Supporting Information.

## Acknowledgements

The computational work was facilitated by access to the UK National Supercomputer, ARCHER (EPSRC Grant EP/L000202) and XSEDE (NSF Grant ACI-1053575). C.M.D. thank the French National Research Agency (ANR project: HOPFAME ANR-13-BS07-0002-01) and acknowledges support from the Fondation de l'Orangerie (Collège de France) for individual Philanthropy

and its donors. Additional support has been received from the Royal Society and the ERC (Grant no. 277757). The IRCELYON thanks its scientific services.

**Keywords:** metal-organic frameworks · mixed linkers · postsynthetic exchange · UV/Vis spectroscopy · UiO-67

- [1] a) J. J. Perry IV, J. a. Perman, M. J. Zaworotko, *Chem. Soc. Rev.* **2009**, *38*, 1400; b) J. R. Long, O. M. Yaghi, *Chem. Soc. Rev.* **2009**, *38*, 1213; c) A. G. Slater, A. I. Cooper, *Science* **2015**, *348*, 8075.
- [2] a) T. Zhang, W. Lin, *Chem. Soc. Rev.* **2014**, *43*, 5982; b) M. C. So, G. P. Wiederrecht, J. E. Mondloch, J. T. Hupp, O. K. Farha, *Chem. Commun.* **2015**, *51*, 3501; c) S. Wang, X. Wang, *Small* **2015**, *11*, 3097.
- [3] a) C. Gomes Silva, I. Luz, F. X. Llabres i Xamena, A. Corma, H. Garcia, *Chem. Eur. J.* **2010**, *16*, 11133; b) S. Pullen, H. Fei, A. Orthaber, S. M. Cohen, S. Ott, *J. Am. Chem. Soc.* **2013**, *135*, 16997; c) D. Sun, Y. Fu, W. Liu, L. Ye, D. Wang, L. Yang, X. Fu, Z. Li, *Chem. Eur. J.* **2013**, *19*, 14279; d) T. Musho, J. Li, N. Wu, *Phys. Chem. Chem. Phys.* **2014**, *16*, 23646; e) T. W. Goh, C. Xiao, R. V. Maligal-Ganesh, X. Li, W. Huang, *Chem. Eng. Sci.* **2015**, *124*, 45; f) C. Wang, Z. Xie, K. E. deKrafft, W. Lin, *J. Am. Chem. Soc.* **2011**, *133*, 13445; g) J. Long, S. Wang, Z. Ding, S. Wang, Y. Zhou, L. Huang, X. Wang, *Chem. Commun.* **2012**, *48*, 11656; h) S. Wang, W. Yao, J. Lin, Z. Ding, X. Wang, *Angew. Chem. Int. Ed.* **2014**, *53*, 1034–1038; *Angew. Chem.* **2014**, *126*, 1052–1056; i) Y. Lee, S. Kim, J. K. Kang, S. M. Cohen, *Chem. Commun.* **2015**, *51*, 5735.
- [4] a) J. H. Cavka, S. Jakobsen, U. Olsbye, N. Guillou, C. Lamberti, S. Bordiga, K. P. Lillerud, *J. Am. Chem. Soc.* **2008**, *130*, 13850; b) M. Kandiah, M. H. Nilsen, S. Usseglio, S. Jakobsen, U. Olsbye, M. Tilset, C. Larabi, E. A. Quadrelli, F. Bonino, K. P. Lillerud, *Chem. Mater.* **2010**, *22*, 6632; c) S. J. Garibay, S. M. Cohen, *Chem. Commun.* **2010**, *46*, 7700; d) A. Schaate, P. Roy, T. Preusse, S. J. Lohmeier, A. Godt, P. Behrens, *Chem. Eur. J.* **2011**, *17*, 9320; e) A. Schaate, S. Duehnen, G. Platz, S. Lilienthal, A. M. Schneider, P. Behrens, *Eur. J. Inorg. Chem.* **2012**, 790; f) Q. Yang, V. Guillerme, F. Ragon, A. D. Wiersum, P. L. Llewellyn, C. Zhong, T. Devic, C. Serre, G. Maurin, *Chem. Commun.* **2012**, *48*, 9831; g) L.-M. Yang, E. Ganz, S. Svelle, M. Tilset, *J. Mater. Chem. C* **2014**, *2*, 7111; h) J. Ethiraj, E. Albanese, B. Civalieri, J. G. Vitillo, F. Bonino, S. Chavan, G. C. Shearer, K. P. Lillerud, S. Bordiga, *ChemSusChem* **2014**, *7*, 3382; i) E. Flage-Larsen, K. Thorshaug, *Inorg. Chem.* **2014**, *53*, 2569; j) A. M. Raseiro-Almansa, A. Corma, M. Iglesias, F. Sanchez, *ChemCatChem* **2014**, *6*, 1794.
- [5] W. A. Maza, R. Padilla, A. J. Morris, *J. Am. Chem. Soc.* **2015**, *137*, 8161.
- [6] a) D. Gianolio, J. G. Vitillo, B. Civalieri, S. Bordiga, U. Olsbye, K. P. Lillerud, L. Valenzano, C. Lamberti, *J. Phys. Conf. Ser.* **2013**, *430*, 012134–012140; b) S. Chavan, J. G. Vitillo, D. Gianolio, O. Zavorotyńska, B. Civalieri, S. Jakobsen, M. H. Nilsen, L. Valenzano, C. Lamberti, K. P. Lillerud, S. Bordiga, *Phys. Chem. Chem. Phys.* **2012**, *14*, 1614–1626; c) L. Valenzano, B. Civalieri, S. Chavan, S. Bordiga, M. H. Nilsen, S. Jakobsen, K. P. Lillerud, C. Lamberti, *Chem. Mater.* **2011**, *23*, 1700–1718.
- [7] L. Li, S. Tang, C. Wang, X. Lv, M. Jiang, H. Wu, X. Zhao, *Chem. Commun.* **2014**, *50*, 2304.
- [8] a) K. Manna, T. Zhang, W. B. Lin, *J. Am. Chem. Soc.* **2014**, *136*, 6566; b) M. I. Gonzalez, E. D. Bloch, J. A. Mason, S. J. Teat, J. P. Long, *Inorg. Chem.* **2015**, *54*, 2995.
- [9] X. Kong, H. Deng, F. Yan, J. Kim, J. A. Swisher, B. Smit, O. M. Yaghi, J. A. Reimer, *Science* **2013**, *341*, 882.
- [10] A. Krajnc, T. Kos, N. Z. Logar, G. Mali, *Angew. Chem. Int. Ed.* **2015**, *54*, 10535–10538; *Angew. Chem.* **2015**, *127*, 10681–10684.
- [11] A. J. Rossini, A. Zagdoun, M. Lelli, J. Canivet, S. Aguado, O. Ouari, P. Tordo, M. Rosay, W. E. Maas, C. Coperet, D. Farrusseng, L. Emsley, A. Lesage, *Angew. Chem. Int. Ed.* **2012**, *51*, 123; *Angew. Chem.* **2012**, *124*, 127.
- [12] A. J. Rossini, L. Emsley, L. A. O'Dell, *Phys. Chem. Chem. Phys.* **2014**, *16*, 12890.
- [13] M. B. Chambers, X. Wang, N. Elgrishi, C. H. Hendon, A. Walsh, J. Bonnefoy, J. Canivet, E. A. Quadrelli, D. Farrusseng, C. Mellot-Draznieks, M. Fontecave, *ChemSusChem* **2015**, *8*, 603.
- [14] S. Øien, D. Wragg, H. Reinsh, S. Svelle, S. Borfiga, C. Lamberti, K. P. Lillerud, *Cryst. Growth Des.* **2014**, *14*, 5370.
- [15] G. Kresse, J. Furthmüller, *Phys. Rev. B* **1996**, *54*, 11169.

- [16] a) J. Heyd, G. E. Scuseria, M. J. Ernzerhof, *Chem. Phys.* **2003**, *118*, 8207; b) J. Heyd, G. E. Scuseria, M. Ernzerhof, *J. Phys. Chem.* **2006**, *124*, 219906.
- [17] a) E. Flage-Larsen, A. Royser, J. Hafizovic Cavka, K. Thorshaug, *J. Phys. Chem. C*, **2013**, *117*, 20610–20616; b) L. M. Yang, E. Ganz, S. Svelle, M. Tilset, *J. Mater. Chem.* **2014**, *24*, 7111–7125; c) S. O. Odoh, C. J. Cramer, D. G. Truhlar, L. Gagliardi, *Chem. Rev.* **2015**, *115*, 6051–6111; d) K. Hendrickx, D. E. P. Vanpoucke, K. Leus, K. Lejaeghere, A. Van Yperen-De Deyne, V. Van Speybroeck, P. Van Der Voort, K. Hemelsoet, *Inorg. Chem.* **2015**, *54*, 10701–10710.
- [18] C. H. Hendon, K. E. Wittering, T.-H. Chen, W. Kaveevivitchai, I. Popov, K. T. Butler, C. C. Wilson, D. L. Cruickshank, O. S. Miljanic, A. Walsh, *Nano Lett.* **2015**, *15*, 2149.
- [19] K. T. Butler, C. H. Hendon, A. Walsh, *ACS Appl. Mater. Interfaces* **2014**, *6*, 22044.
- [20] J. Heine, K. Mueller-Buschbaum, *Chem. Soc. Rev.* **2013**, *42*, 9232.

---

Received: January 12, 2016

Published online on February 2, 2016